Reduced order model based metamodeling for multiparametric local heat treatment simulations

Leonardo Cimatti Lucarelli, Nawfal Blal, Anthony Gravouil, Auriane Platzer, David Iampietro, Josselin Delmas, Thomas Potin

CSMA 2024
16ème Colloque National en Calcul des Structures
13-17 Mai 2024, Presqu'île de Giens (Var)

Reduced order model based metamodeling for multiparametric local heat treatment simulations

L. Cimatti Lucarelli[1], N. Blal[1], A. Gravouil[1], A. Platzer[1], D. Iampietro[2],
J. Delmas[2], T. Potin[3]

[1] *LaMCoS, INSA de Lyon, {leonardo.cimatti-lucarelli, nawfal.blal, anthony.gravouil, auriane.platzer}@insa-lyon.fr*
[2] *EDF R&D, {david.iampietro, josselin.delmas}@edf.fr*
[3] *Framatome DTI, thomas.potin@framatome.com*

Abstract —
The objective of the present work is to combine reduced order model (ROM) methods with parameter-to-solution metamodeling techniques to predict instantly the mechanical state at the end of Post Welding Heat Treatments on industrial steel pipelines. The ROM method used is based on a proper orthogonal decomposition (POD) and Grassmann interpolation strategy with parametric finite elements simulations. Additionally to the accuracy estimation of the resulting surrogate model, global variance and sensitivity analysis are carried out to determine operation parameters influence qualitative and quantitative.
Keywords — thermomechanical simulation, Metamodeling, POD, Post Welding Heat Treatments.

1 Introduction

Post welding heat treatments (PWHT) technique are largely used in many industrial sectors such as petrochemical ([1], [2], [3], [4]), nuclear power plants ([5]), automotive([6]), among others. This kind of heat treatment made after welding operations, aims to relax residual stresses and enhance some mechanical properties (fracture toughness, yield strength, among others). Consequently, such industrial process prevent early maintenance, reduction of equipment lifetime and ensure correct functioning during service.
The success of a PWHT on large steel pipelines strongly depends on the capacity to impose and control the appropriate thermal load at the material core. Over or under heating during the operation may be responsible for not relaxing sufficiently the equipment or depreciating its mechanical properties. Other PWHT conditions may affect its results, such as uncontrolled thermal gradients and asymmetrical pipelines, reducing the heat treatment efficiency. In order to estimate the influence of these different thermal and operations conditions, a parametric finite element model was created to generate a surrogate model based on POD and Grassmann interpolation method and a global analysis of PWHT.
With this metamodeling and interpolation strategy it is possible to generate rapidly, entire fields of result to stress and strain field with a controlled interpolation error.

2 Material behavior and constitutive laws

Stress relaxation during PWHT may be triggered by two mechanisms. The first one is related to a decrease in Young modulus and yield strength for metallic materials as temperature increases, and as consequence a stress relaxation. The amount of relaxed stress by this mechanism is a function of the difference of the ration between these two mechanical properties, shown in [1]. The second mechanism is the viscoplastic behavior for temperatures above one third of the fusion temperature in metals. It differs from plastic behavior as it depends on both the strain (as in plastic behavior) and the strain rate, it is also known as rate dependent inelastic behavior ([7]).
In the context of PWHT in steel equipment and pipelines, it is important to model the inelastic behavior of the material in low temperatures, presenting a plastic behavior, as well as in higher temperatures, presenting a viscoplastic behavior. In the present work, the target material is a low alloy ferritic steel, commonly referred to as 16MND5 or A508 Cl3 by industrial stakeholders. Such steel grade is largely used in nuclear power plants installations, such as bottom vessel of steam generators. Vincent [8] de-

scribed the material behavior of this steel grade during both welding and PWHT simulations, showing a good match for residual stress between experimental and simulation results.
The modeling of this steel behavior consists in a mixed law: for lower temperatures it is a plastic non-linear isotropic hardening and for higher temperatures it is a viscoplastic non-linear isotropic hardening. The constitutive equations as well as the state potential (here Helmholtz free energy) and dissipation potential are as described in sections bellow.

2.1 State potential and thermomechanical laws

The state potential for an isotropic material, such as the steel in the current work, with temperature variation to model and the respective thermodynamic forces definitions for $\boldsymbol{\sigma}$ and R are given by equations 1. It can be underlined that both plastic and viscoplastic behaviors have the same state potential and thermoelastic laws.

$$\begin{cases} \Psi(\varepsilon^{\text{tot}}, \varepsilon^{\text{ine}}, p) = \frac{1}{2\rho}(\varepsilon^{\text{tot}} - \varepsilon^{\text{ine}} - \varepsilon^{\text{ther}}) : \mathbb{C} : (\varepsilon^{\text{tot}} - \varepsilon^{\text{ine}} - \varepsilon^{\text{ther}}) + \frac{1}{\rho} R_\infty (p + \frac{1}{b}(e^{-bp} - 1)), \\ \boldsymbol{\sigma} = \rho \frac{\partial \Psi}{\partial \boldsymbol{\epsilon}^e} = \mathbb{C} : (\varepsilon^{\text{tot}} - \varepsilon^{\text{ine}} - \varepsilon^{\text{ther}}), \\ R = \rho \frac{\partial \Psi}{\partial p} = R_\infty (1 - e^{-bp}), \\ \boldsymbol{\epsilon}^{\text{ther}} = \alpha \theta \mathbf{I} \end{cases} \tag{1}$$

where the thermodynamical forces are $\boldsymbol{\sigma}$ (stress tensor) and non-conservative force R, $\boldsymbol{\epsilon}$ (resp. $\boldsymbol{\epsilon}^{\text{ine}}$) is the total (resp. inelastic) strain tensor, $\boldsymbol{\epsilon}^{\text{ther}}$ is the thermal strain, the internal variable p corresponds to the accumulated inelastic strain, $\mathbb{C}$ is the Hook tensor, R_∞ and b are material parameters, α is the dilatation coefficient, θ is the temperature minus the reference temperature, and $\mathbf{I}$ is the identity matrix.

2.2 Dissipation potential and dissipative laws

For plastic behavior, the definitions of the yield surface, as well as the normal dissipative laws for the accumulated inelastic strain p and the inelastic strain $\boldsymbol{\epsilon}^{in}$ are given by equations 2:

$$Plastic : \begin{cases} \varphi^*_{vp}(\boldsymbol{\sigma}, R) = \mathbb{I}_f(\sigma, R), \text{ with } f(\boldsymbol{\sigma}, R) = \|\boldsymbol{\sigma}\|_{vM} - R - \sigma_y \leq 0 \\ \dot{\boldsymbol{\epsilon}}^{in} = \lambda \frac{\partial f}{\partial \boldsymbol{\sigma}} \\ \dot{p} = -\lambda \frac{\partial f}{\partial R} = \lambda \end{cases} \tag{2}$$

where $\mathbb{I}_f$ is the indicator function of f, f is the yield surface, and λ is a plasticity multiplier.
For viscoplastic behavior the definitions of dissipation potential, the normal dissipative laws for accumulated inelastic strain and inelastic strain respectively are given by equations 3:

$$Viscoplastic : \begin{cases} \varphi^*_{vp}(\boldsymbol{\sigma}, R) = \frac{K}{n+1} \left\langle \frac{\|\boldsymbol{\sigma}\|_{vM} - R - \sigma_y}{K} \right\rangle^{n+1} \\ \dot{\boldsymbol{\epsilon}}^{in} = \dot{p} \frac{3}{2} \frac{\boldsymbol{\sigma}^{\text{dev}}}{\|\boldsymbol{\sigma}^{\text{dev}}\|_{vM}} \\ \dot{p} = \left\langle \frac{\|\boldsymbol{\sigma}\|_{vM} - R - \sigma_y}{K} \right\rangle^{n} \end{cases} \tag{3}$$

where n and K are material parameters, and $\langle \cdot \rangle = \max(0, \cdot)$.
This material behavior system of equations is implemented in *Code_Aster* ([9]) a thermomechanics finite elements simulation software developed by EDF R&D. The time integration of material law has been implemented with *MFront*([10]) which can be easily interfaced with *Code_Aster*.

3 Parametric model and model reduction strategy

3.1 Parametric model

The application case of the current work consists in making a local PWHT on a pipeline, presented in Figure 5a. This geometry is represented by a 2D axisymmetric rectangle, presented in Figure 5c,

where $\boldsymbol{y}$ is a revolution axis and the plan $(\boldsymbol{x}, \boldsymbol{z})$ represents the center of the welding center line and a symmetry plan. As indicated in Figure 5c, there are three zones in a local PWHT operation, the soak band corresponds to the zone where the initial stresses should be relaxed and is the zone closer to the welding center-line, the heating band is the zone that will be heated to attain the target temperature during PWHT. Finally, the gradient control band is where the thermal gradient is controlled to avoid generating excessive and additional stresses zones during PWHT.
The temperature cycle, zones sizes, cooling and heating time are defined in european and international standards and codes for engineering practices (WRC 452/552 ([11], [12]), AWS D10.10 ([13]), RCC-M S1340/ S7450 ([14])). Figure 2 displays the characteristic shape of a temperature time cycle during PWHT as well as its admissible range of variations according to WRC Table 1, where t is the thickness, and R is the internal radius.

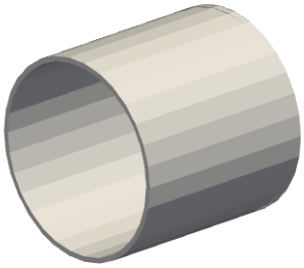

(a) Pipeline geometry representation

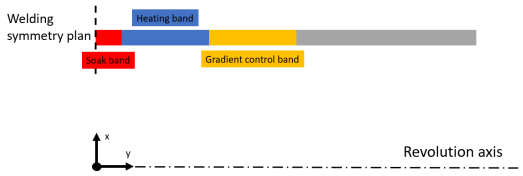

(b) Different zones in PWHT norms

Figure 1: Pipeline axisymmetric and 3D representation + PWHT Zones

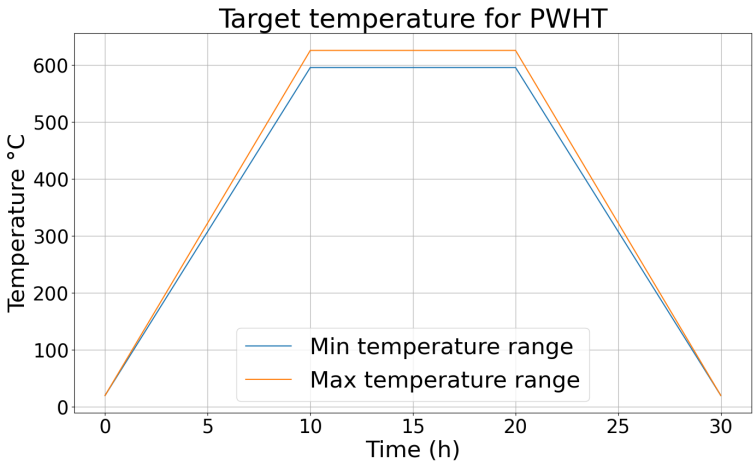

Figure 2: Temperature range in PWHT - WRC recommendation

Table 1: Preconized values of PWHT zone lengths on WRC norm

Zone name	Zone value
Soak band	t
Heating band	$t+2\sqrt{Rt}$
Gradient control band	$t+2\sqrt{Rt}$

As it can be noticed, several operation parameters, such as *max_temp* the target temperature, $\dot{T}_{heating}$

the heating rate, $\dot{T}_{cooling}$ the cooling rate, t_{hold} the hold time, *l_max_temp* the heating band length and *l_grad_temp* the gradient control length, can be already identified.
In the present work these parameters vary $\pm 15\%$ from the values defined in engineering standards and codes. The material behavior is described in the section above and the FE simulations have been carried out with *Code_Aster*.

3.2 Model reduction strategy

3.2.1 PDO + Grassmann design

There are plenty of model reduction techniques available such as POD (Proper Orthogonal Decomposition), neural networks autoencoders, PGD (proper generalized decomposition), kringing, PCE, piecewise polynomial metamodels, among others. However not all of them are appropriated for thermomechanical applications.
The present work uses a proper orthogonal decomposition combined with a Grassmann interpolation to adapt reduced modes. This approach has already shown promising results for mechanical and thermomechanical parametric metamodeling ([15], [16]). POD and Grassmann interpolation strategy relies on calculating simulation snapshots and interpolating its orthogonal bases for new operation parameters that have not been previously computed.
The Grassmann interpolation method requires the notion of Grassmann manifold represented as a spining circle in Figure 3. On this circle, two reduced basis Ψ_0 and Ψ_1 are represented. They are related to two different set of operation parameters. The Grassmann interpolation allows to compute an intermediary reduced basis, $\Psi_{interpol}$, when the parameter vector changes. Its main advantage is that it takes into account the non-linearity of the manifold as the parameter inputs vary. In order to do so, it relies on the computation of two operators: the Exp mapping and the Log mapping.

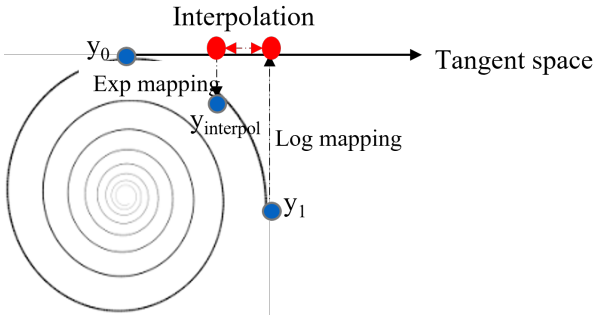

Figure 3: Grassmann interpolation representation

The projection of Ψ_1 in the tangent space of the reference basis, Ψ_0, is named logarithmic mapping. Given in equation 4 ([16]), U_{log}, Σ_{log}, and V_{log} are the resulting matrices of the thin SVD decomposition of the resulting matrix written of the left-hand side of the equality, and Γ is the projection of Ψ_1 into the tangent space of Ψ_0.

$$\begin{aligned}(I-\Psi_0\Psi_0^T)\Psi_1(\Psi_0^T\Psi_1)^{-1} &= U_{log}\Sigma_{log}V_{log}^T \\ \Gamma &= U_{log}\tan^{-1}(\Sigma_{log})V_{log}^T\end{aligned} \tag{4}$$

Once Φ_1 is projected on the Φ_0 tangent space, a linear input parameter interpolation can be performed as this space is linear.
The interpolated basis is then projected into the original space using the exponential mapping ([16]). Given in equation 5, where U_{exp}, Σ_{exp}, and V_{exp} are the thin SVD decomposition of the interpolated basis in the tangent space of Ψ_0, and $\Psi_{interpol}$ is the final result of the interpolation at the original space.

$$\begin{aligned}\Gamma &= U_{exp}\Sigma_{exp}V_{exp}^T \\ \Psi_{interpol} &= (\Psi_0 V_{exp}\cos(\Sigma_{exp}) + U_{exp}\sin(\Sigma_{exp}))V_{exp}^T\end{aligned} \tag{5}$$

The main advantages of the Grassmann interpolation method with respect to standard linear matrix interpolation area that the resulting base is orthogonal, and that the interpolation is made in a non-linear

space. What is more, the reduction of the interpolation error will be faster using this method for complex non-linear problems such as simulations with viscoplastic and plastic material behavior.

3.2.2 Multigrid localized error sampling

The developed algorithm is applied to a domain in the parametric space. The first step is to produce snapshots at the corners of the parametric domain and at the center of the domain. The Grassmann interpolation step is performed using the reduced basis obtained with POD from corner parameters. The interpolation is done for a parameter value corresponding to the center of the hypercube and is used to compute the interpolation error. If the error is superior to the tolerance, the space is subdivided in other hypercubes, and the initial step restarts for each subspace created in division of the original hypercube. This subdivision and error computation is automatic until every subspace of the original domain has converged to an error smaller than the tolerance. Lu et al. [15], proposed this localized sparse grid technique for parametric welding simulations.
The algorithm adapts to produce more snapshots where the convergence is more difficult. Figure 4 gives an example of converged space for two parameters. One may see that there are zones where the parameter cubic grid has been considerably refined meaning that a large number of snapshots have been computed. Only the snapshots used in interpolation are represented.

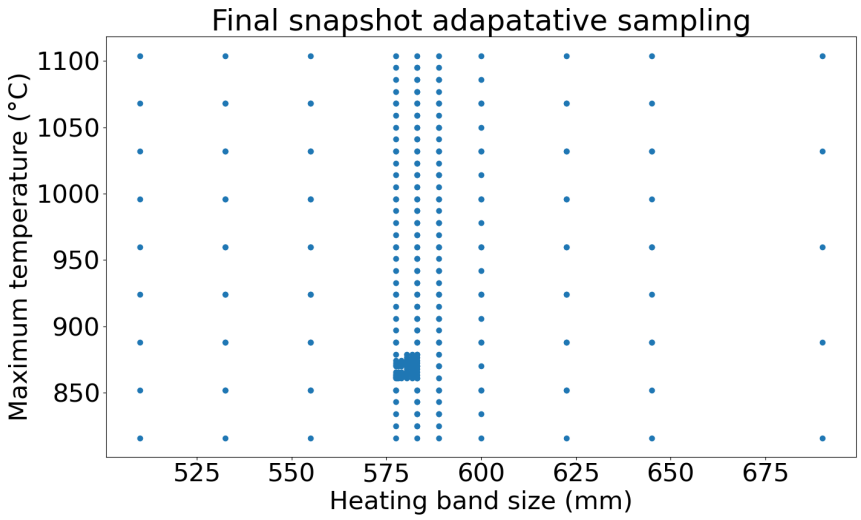

Figure 4: Converged snapshots for adaptive algorithm

3.3 Sensitivity analysis for PWHT

Constructing the surrogate model for PWHT allows making sensitivity analysis and take conclusions that may impact an industrial operation design in terms of parameters values, or even determine what are the most influential parameters to stress relaxation. The following results were generated for an application with 2 parameters the targer temperature *max_temp* and the heating band length *l_max_temp*.
In Figure 5 the Sobol index for the 2 parameters and 3 quantities of interest, the maximum von Mises stress at the soak band, the maximum von Mises stress at the entire component and the distance of this point to the symmetry plan (welding center-line). The temperature applied for the heat treatment is more influential for all quantities of interest compared to the length of the heating band.
Another important analysis that may be easily made with a surrogate model that produces instantaneous results is presented Figure 6, here the maximum von Mises stress at the soak band and at the entire component in function of the temperature the heat treatment is performed. Until $550°C$ the maximum stress is at located at the soak band. As one of the goals of PWHT is to relax the stress near welded area a heat treatment should be performed in temperatures higher than $550°C$.

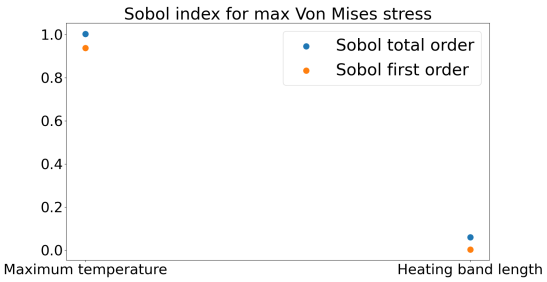

(a) Sobol index of maximum von Mises stress value

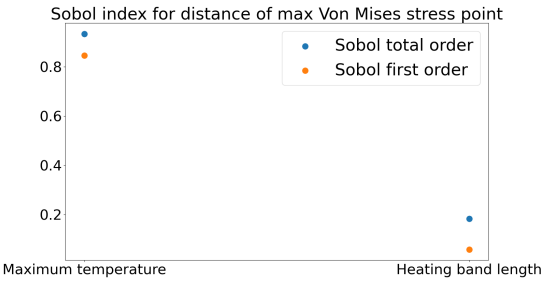

(b) Sobol index of distance of the maximum von Mises stress value to welding center

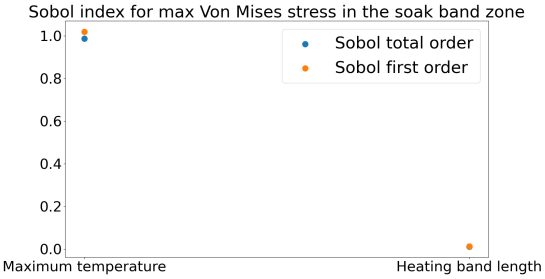

(c) Sobol index to maximum von Mises stress at the soak band

Figure 5: Sobol index for 3 quantities of interest

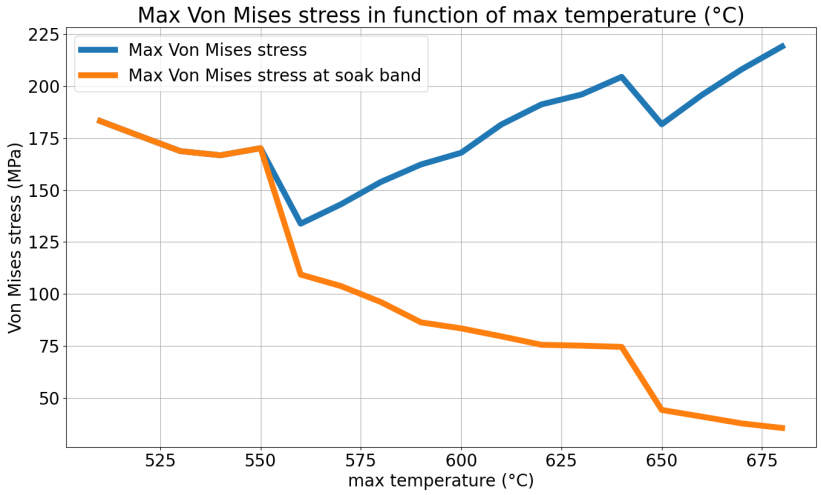

Figure 6: Max von Mises stress at the soak band and entire component in function of heat treatment temperature

4 Conclusion and perspectives

In summary a surrogate model of FE parametric model of post-welding heat treatment was made and multiple snapshots results were taken. The surrogate model was built using POD and Grassmann interpolation method, using this surrogate model several global sensitivity analysis can possibly be made. In the future other ROM-based metamodels will be developed coupling HOPGD ([17], [18], [19]) method with physically based corrections.

5 Acknowledgments

The authors gratefully acknowledge the support from the joint laboratory "Soudage & Réparation", a collaboration between Électricité de France (EDF), Framatome and INSA Lyon.

References

[1] Pingsha Dong, Shaopin Song, and Jinmiao Zhang. Analysis of residual stress relief mechanisms in post-weld heat treatment. *International Journal of Pressure Vessels and Piping*, 122:6–14, October 2014.

[2] Qiang Jin, Wenchun Jiang, Wenbin Gu, Jinguang Wang, Gang Li, Xiaodong Pan, Ming Song, Kai Zhang, Aibing Wu, and Shan-Tung Tu. A primary plus secondary local PWHT method for mitigating weld residual stresses in pressure vessels. *International Journal of Pressure Vessels and Piping*, 192:104431, August 2021.

[3] Qiang Jin, Wenchun Jiang, Chengcai Wang, Zhongwei Yang, Yun Luo, Guizhen Yan, Shan-Tung Tu, and Yinbiao He. A rigid-flexible coordinated method to control weld residual stress and deformation during local PWHT for ultra-large pressure vessels. *International Journal of Pressure Vessels and Piping*, 191:104323, June 2021.

[4] Hakan Aydın, Ali Bayram, and İsmail Durgun. The effect of post-weld heat treatment on the mechanical properties of 2024-T4 friction stir-welded joints. *Materials & Design (1980-2015)*, 31(5):2568–2577, May 2010.

[5] Junyeong Kim, Jong-Hun Kim, Jungsoo Park, Seungyeop Baek, Ninshu Ma, Seung-Joon Lee, and Dongjin Kim. Continuous tempering effect induced PWHT alternative technology using wire arc additive manufacturing for application in replacing nuclear pressurized water reactor system repairing: CALPHAD, FEM simulation, and EBSD investigation. *Journal of Materials Research and Technology*, 25:2961–2988, July 2023.

[6] Henrik Alberg. *Simulation of Welding and Heat Treatment: Modelling and Validation*. PhD thesis.

[7] Lemaître Jean and Chaboche Jean-Louis. *Mécanique des matériaux solides*. Dunod, Paris, France, 2 edition, 2004.

[8] Yannick Vincent. *Simulation numérique des conséquences métallurgiques et mécaniques induites par une opération de soudage : acier 16MND5*. PhD thesis, 2002. Thèse de doctorat dirigée par Gilles, Philippe et Jullien, Jean-François Génie civil Lyon, INSA 2002.

[9] Electricité de France. Finite element code_aster, Structures and Thermo- mechanics Analysis for Studies and Research, 1989.

[10] Thomas Helfer, Bruno Michel, Jean-Michel Proix, Maxime Salvo, Jérôme Sercombe, and Michel Casella. Introducing the open-source mfront code generator: Application to mechanical behaviours and material knowledge management within the PLEIADES fuel element modelling platform. *Computers & Mathematics with Applications*, 70(5):994–1023, September 2015.

[11] Welding Research Council Bulletin. WRC 452 - Welding Research Council Bulletin - Recommended Practices for local heating of welds in pressure vessels, june 2000., June 2000.

[12] Welding Research Council (U.S.). WRC 552 - Welding Research Council Bulletin - Calculation of weld residual stresses and the effects of Local Post-Weld Heat Treatment., 2016.

[13] AWS - American welding society. AWS D10.10 - AWS D10.10 - American Welding Society - American National Standrard Institute- Recommended Practices for Local Heating of welded in Piping and Tubing., 2021.

[14] Association française pour les règles de conception, de construction et de surveillance en exploitation des matériels des chaudières électro-nucléaires. RCC-M S1340 and S7540 - Edition 2018 - Règles de Conception et de Construction des Matériels mécaniques des îlots nucléaires REP., 2018.

[15] Y. Lu, N. Blal, and A. Gravouil. Space–time POD based computational vademecums for parametric studies: application to thermo-mechanical problems. *Advanced Modeling and Simulation in Engineering Sciences*, 5(1):3, February 2018.

[16] David Amsallem and Charbel Farhat. Interpolation Method for Adapting Reduced-Order Models and Application to Aeroelasticity. *AIAA Journal*, 46(7):1803–1813, July 2008.

[17] Rubén Ibáñez, Emmanuelle Abisset-Chavanne, Amine Ammar, David González, Elías Cueto, Antonio Huerta, Jean Louis Duval, and Francisco Chinesta. A Multidimensional Data-Driven Sparse Identification Technique: The Sparse Proper Generalized Decomposition. *Complexity*, 2018:e5608286, November 2018.

[18] Y. Lu, N. Blal, and A. Gravouil. Datadriven HOPGD based computational vademecum for welding parameter identification. *Computational Mechanics*, 64(1):47–62, July 2019.

[19] Y. Lu, N. Blal, and A. Gravouil. Adaptive sparse grid based HOPGD: Toward a nonintrusive strategy for constructing space-time welding *computational vademecum*. *International Journal for Numerical Methods in Engineering*, 114(13):1438–1461, June 2018.